EVOLUTIONARY HIGHWAYS TO PERSISTENT BACTERIAL INFECTION

Jennifer A Bartell[1,*,§], Lea M Sommer[2,*], Janus A J Haagensen[1], Anne Loch[1], Rocio Espinosa[1], Søren Molin[1], and Helle Krogh Johansen[2,3]

[1]The Novo Nordisk Foundation Center for Biosustainability, Technical University of Denmark, 2800 Kgs. Lyngby, Denmark.

[2]Department of Clinical Microbiology, Rigshospitalet, 2100 Copenhagen Ø, Denmark.

[3]Department of Clinical Medicine, Faculty of Health and Medical Sciences, University of Copenhagen, Copenhagen, Denmark.

*Corresponding authors and equal contribution

[§]Lead contact

KEYWORDS

Evolution; Persistent Infection; Antibiotic Resistance; Cystic fibrosis; *Pseudomonas aeruginosa*; Clinical Isolates; Longitudinal Analysis; Data Modeling; Genotype-Phenotype

ABSTRACT

Persistent infections require bacteria to evolve from their naïve colonization state by optimizing fitness in the host. This optimization involves coordinated adaptation of multiple traits, obscuring evolutionary trends and complicating infection management. Accordingly, we screen 8 infection-relevant phenotypes of 443 longitudinal *Pseudomonas aeruginosa* isolates from 39 young cystic fibrosis patients over 10 years. Using statistical modeling, we map evolutionary trajectories and identify trait correlations accounting for patient-specific influences. By integrating previous genetic analyses of 474 isolates, we provide a window into early adaptation to the host, finding: 1) a 2-3 year timeline of rapid adaptation after

colonization, 2) variant "naïve" and "adapted" states reflecting discordance between phenotypic and genetic adaptation, 3) adaptive trajectories leading to persistent infection via 3 distinct evolutionary modes, and 4) new associations between phenotypes and pathoadaptive mutations. Ultimately, we effectively deconvolute complex trait adaptation, offering a framework for evolutionary studies and precision medicine in clinical microbiology.

Bacteria have spent millennia evolving complex and resilient modes of adaptation to new environments, and some species effectively deploy these skills as pathogens during colonization and persistence within human hosts[1–3]. Due to gradual increases in fitness via accumulating genetic and epigenetic changes, it has been difficult to pinpoint overarching drivers of adaptation (from systems-level traits down to individual mutations) that reliably signal fitness [Leon et al. 2018]. Distinct populations may travel along the same predictable path to successful persistence, but other unique sequences of multi-trait adaptation can be equally optimal[4] in a complex, fluctuating environment[5]. This is even more relevant in a clinical context where dynamic selection pressures are applied via therapeutic treatment intended to eradicate infection.

Even for a well-studied model system of bacterial persistence and chronic infection such as the airway infections of cystic fibrosis (CF) patients, evolutionary trajectories remain difficult to map due in part to competing modes of evolution. We know from laboratory evolution studies in highly controlled conditions that these multiple modes are at work and induce substantial phenotypic adaptation to minimal media within the initial 5,000-10,000 generations[6–8], but only an estimate is available of the timeline of adaptation in the complex CF lung environment[9]. Multiple recent studies have shown a high degree of population heterogeneity in chronic CF infections that could be influenced by competing evolutionary modes, but past consensus has been that select traits converge torwards similar “evolved” states during most CF infections (e.g. loss of virulence and increase in antibiotic resistance)[3,10–12]. This convergence can be complex and drug-driven, as recent studies have shown development of collateral sensitivity to antibiotics (treatment with one drug can induce reciprocal changes in sensitivity to other drugs)[13]; this illustrates that a single selection

pressure can reversibly affect multiple other traits, obscuring evolutionary trends. Bacterial infections of CF airways are thus influenced by strong and competing selective forces from very early in a patient's life, but few studies have focused on the early periods of infection where environmental strains transition to successful pathogens in patient lungs.

Studies have assessed the genetic evolution of human pathogens and identified specific genetic adaptations correlating with colonization and persistence[14–16]. However, only a few have linked genotypic and phenotypic changes[2,9,17,18], as this is especially challenging in natural populations. The genetic signature of adapting phenotypes is obscured over the course of evolution by the continuous accumulation of mutations and acclimatization by environment-based tuning of pathogen activity. Furthermore, it is inherently difficult to identify genotype-phenotype links for complex traits governed by multiple regulatory networks[19,20]. Consequently, we are far from the reliable prediction of phenotypic adaptation by mutations alone during evolution in a complex, dynamic environment[19,21], and we propose that for now, phenotypic characterization is equally important.

To address the complexity of pathogen adaptation in the host environment, we analyzed our phenotypic dataset using statistical methods that account for the environmental effects on patient-specific lineages (Generalized Additive Mixed Models – GAMMs) and assess adaptive paths traversing the evolutionary landscape from a multi-trait perspective (Archetype Analysis – AA). We identify emergent patterns of bacterial phenotypic change across our patient cohort that depart from expected evolutionary paths and estimate the period of initial rapid adaptation during which the bacteria transition from a "naïve" to an "evolved" phenotypic state. We further identify distinct and repeating trajectories of pathogen evolution, and by leveraging our prior genomics study of this isolate collection[16], we propose new associations between these phenotypic phenomena and genetic adaptation. We find that specific traits, such as growth rate and ciprofloxacin resistance, can serve as rough estimators of adaptation in our patients, while multi-trait modeling can map complex, patient-specific trajectories towards distinct evolutionary optimums that enable persistence. Implementation of this trajectory modeling as a diagnostic tool in patient care might enable clinicians to respond more quickly and effectively to evolving pathogens and inhibit the transition to a persistent infection.

91

92 # RESULTS

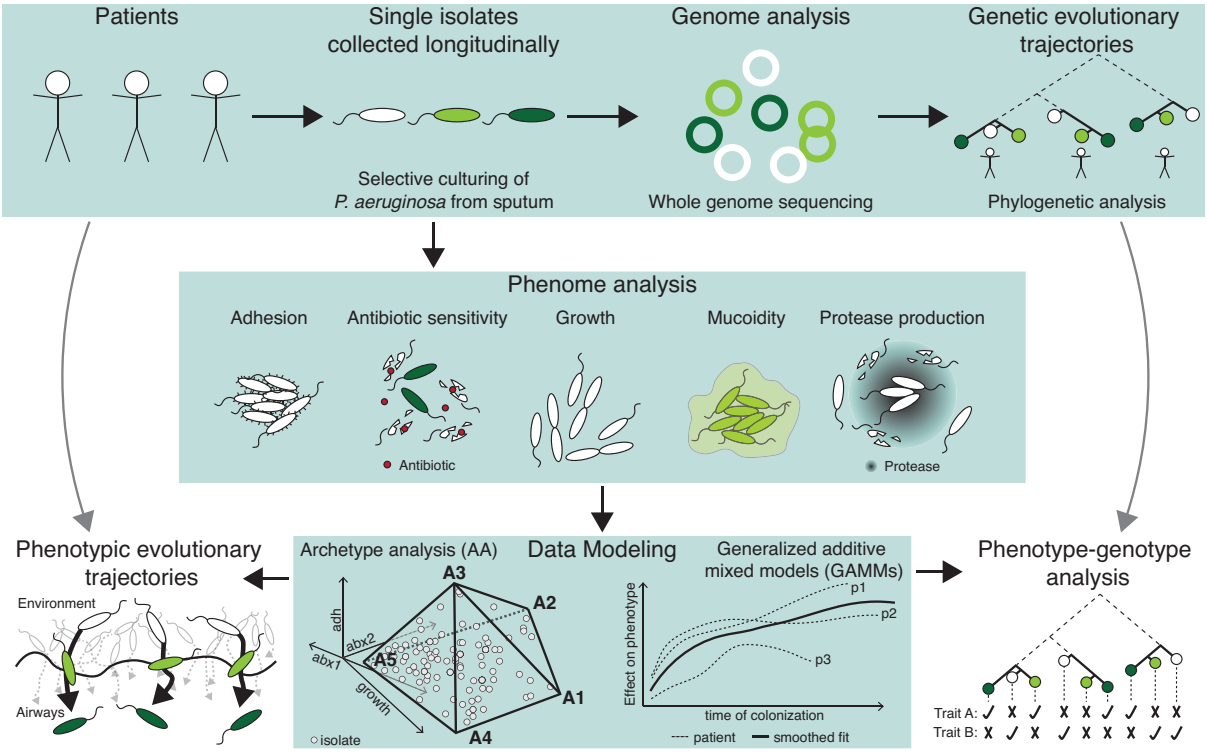

93

Figure 1. *Study design.* **Upper panel:** Every month, CF patients are seen at the CF clinic at Rigshospitalet in Copenhagen, Denmark. Here they deliver a sputum or endolaryngeal suction sample where selective microbiological culturing is performed[76]. The longitudinally collected isolates have been genome sequenced and analyzed previously[16]. **Middle panel:** Longitudinally collected isolates have been subjected to different phenotypic analyses for this study and are here (**lower panel**) analyzed using two data modelling approaches: Archetype Analysis (AA) and Generalized Additive Mixed Model (GAMM). By integrating these approaches, we map dominant evolutionary trajectories and analyze mechanistic links between phenotypic and genetic adaptation.

94

95 ## Evaluating pathogen adaptation in the early stage of infection

96 *A unique dataset.* The 443 clinical *P. aeruginosa* isolates originate from a cohort of 39 youth
97 with CF (median age at first *P. aeruginosa* isolate = 8.1 years) treated at the Copenhagen CF
98 Centre at Rigshospitalet and capture the early period of adaptation, spanning 0.2-10.2 years
99 of colonization by a total of 52 clone types. Of these isolates, 373 were previously
100 characterized in a molecular study of adaptation[16]. The "colonization time of an isolate" (ColT)
101 is defined for each specific lineage, approximating the length of time since a given clone type
102 began colonization of the CF airways in the specific patient. Importantly, our colonization time
103 metric does not necessarily start at the true "time zero", since a significant bacterial load is
104 necessary for a positive culture. Our isolate collection also does not capture the complete

105 population structure, but a previous study shows that 75% of our patients have a monoclonal
106 infection persisting for years with mutations accumulating in a highly parsimonious fashion
107 indicating unidirectional evolution[16]. Additionally, a metagenomic study of 4 patients from
108 our cohort indicates that the single longitudinal isolates are representative of the major
109 propagating subpopulation[22].
110
111 To obtain systems-level readouts of pathogen adaptation in the host and thereby assess
112 multi-trait evolutionary trajectories, we present an infection-relevant characterization of our
113 isolate collection entailing high-throughput measurements of 8 phenotypes: growth rates (in
114 Luria-Bertani broth (LB) and Artificial Sputum Medium (ASM)), antibiotic susceptibility (to
115 ciprofloxacin and aztreonam), virulence factors (protease production and mucoidity), and
116 adherence (adhesion and aggregation) (Figure 1 and 2). We define adherence as a shared
117 trend in adhesion and aggregation which we associate with a biofilm-like lifestyle (see
118 Methods for further discussion of limitations of these measures). These phenotypes are
119 generally accepted to change over the course of colonization and infection of CF airways
120 based primarily on studies of chronically-infected patients[10,17,23,24].
121
122 That is, an "evolved" isolate would grow slowly, adhere proficiently, be more likely to exhibit
123 a mucoid and/or hypermutator phenotype, have reduced protease production, and resist
124 antibiotics, in contrast to a "naïve" isolate (Figure 2B). However, simply ordering our
125 measurements by colonization time does not illustrate an overarching adaptive trajectory
126 from naïve to evolved phenotypes (Figure 2C). Instead, we see substantial heterogeneity, with
127 isolates that resemble both naïve and evolved phenotypic states throughout the study period.
128 Given that we are investigating a unique collection from a young patient cohort that we track
129 for a substantial period of colonization, this data fills the critical gap between studies of acute
130 infections and chronic infections[25]. We are surprised to see naïve phenotypes retained in late
131 colonization as well as isolates in early colonization that deviate significantly from PAO1
132 phenotypes. However, a general pattern of heterogeneity is in alignment with previous
133 studies of both *P. aeruginosa* and *Burkholderia* spp. infections[3,11,12].
134

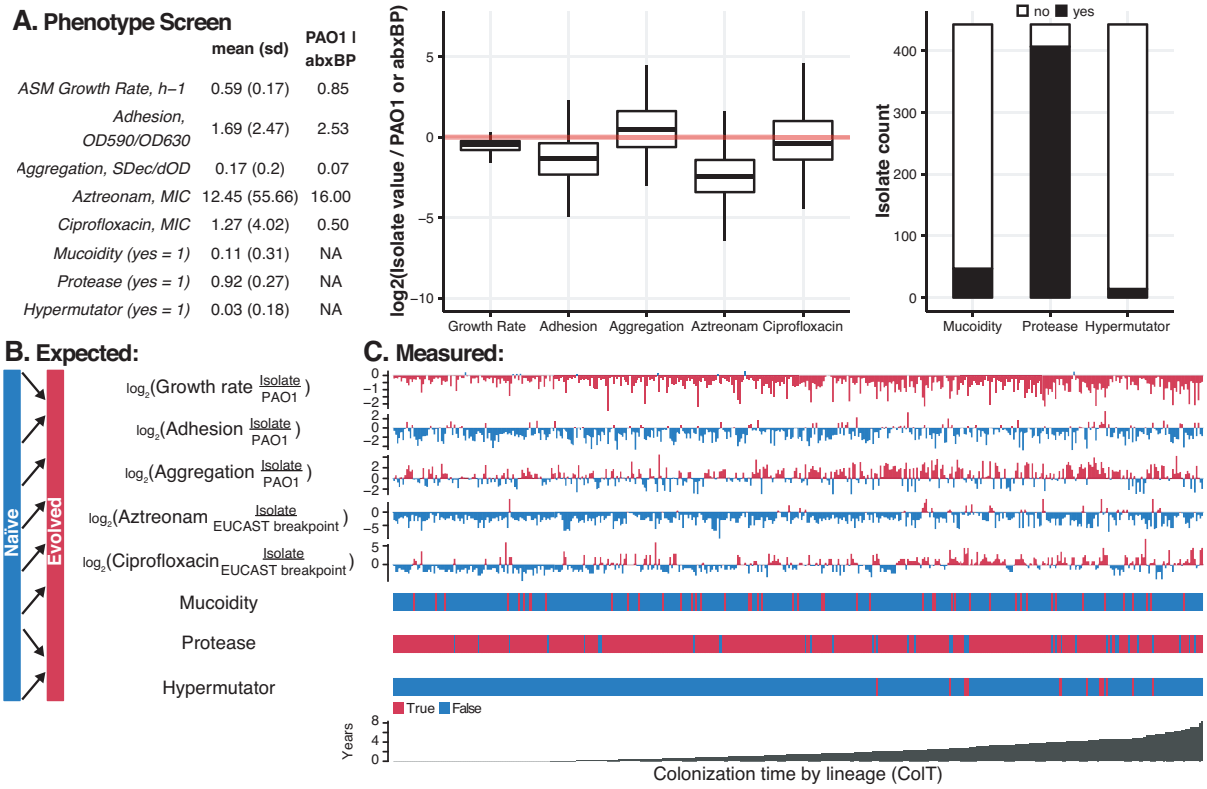

Figure 2. *Phenotypic characterization.* We present summary statistics of our phenotype screen including **(A)** mean and standard deviation of isolate data versus the *P. aeruginosa* PAO1 value or antibiotic breakpoint we use for normalization, respectively, as well as boxplots of continuous variables (showing the median, 1st and 3rd quartile hinges, whiskers extending from the hinges to the most extant value within 1.5x inter-quartile range, and outliers as points). We then compare the **(B)** expected adaptation over time based on field consensus versus **(C)** the measured raw adaptation of our isolate collection over time. After sorting the isolates (x-axis) by the time since colonization of a specific lineage or "colonization time" (ColT), it is still difficult to see consistent patterns of phenotypic change over time. Colors are linked with the expected change of the specific phenotype (B), so that blue denotes a "naïve" phenotype and red denotes an "evolved" phenotype. For growth rate (in artificial sputum medium (ASM)), adhesion, and aggregation, naïve and evolved phenotypes are roughly divided by comparison with the reference isolate PAO1 phenotype. For aztreonam and ciprofloxacin MIC, naïve and evolved phenotypes are based on sensitivity or resistance as indicated by the EUCAST breakpoint values as of March 2017.

A unique modeling approach. Because our data is heterogeneous, we required specialized modeling approaches to account for specific environmental pressures and assess the boundaries of the evolutionary landscape. Previous studies have employed linear mixed models of phenotypic adaptation[26], and employed archetype analysis in the comparison of features of transcriptomic adaptation by *P. aeruginosa*[27]. Similar studies of multi-trait evolutionary trade-offs using polytope fitting have predicted the genetic polymorphism structure in a population[28]. We use related modeling methods to ensure that patient-specific effects are minimized, irregular sampling intervals are smoothed and a multi-trait perspective is prioritized by 1) modeling the dynamic landscape of multi-trait evolution using AA and 2) evaluating temporal correlations of phenotypic adaptation by fitting cross-patient trendlines

147 using GAMMs (Figure 1). We describe our approach below in brief, with more extended
148 explanation available in both the Methods and Supplements 1 and 2.
149
150 With AA, we want to assess multi-trait adaptive paths within the context of the evolutionary
151 landscape. We map these paths (or trajectories) by first fitting idealized extreme isolates
152 ("archetypes") located on the boundaries of the evolutionary landscape and then evaluating
153 every other isolate according to its similarity to these idealized extremes. The archetypes are
154 positioned at the "corners" of the principal convex hull (PCH), the polytope of minimal volume
155 that effectively encapsulates our phenotype dataset[29] (Figure 1, bottom panel). We
156 conceptualize archetypes as the "naïve" and "evolved" states of plausible adaptive
157 trajectories and predict both the optimal number of archetypes and their distinct phenotypic
158 profiles. We illustrate the AA by the 2D projection of our multi-trait model via a "simplex"
159 plot, as shown in Figure 3C[30].
160
161 With the GAMMs, we want to predict whether a given phenotype (the "predicted" variable)
162 significantly correlates with other phenotypes or time (the "explanatory" variables). To do
163 this we need to account for the effects of patient specific environments and the effect of
164 sampling time, while fitting trend lines for each trait (Figure 1, bottom panel). This is done by
165 fitting patient and time as random effects; we reduce the risk of overfitting by using a
166 penalized regression spline approach with smoothing optimization via restricted maximum
167 likelihood (REML)[31]. To avoid assumptions of "cause-and-effect" between our variables, we
168 permute through different one-to-one models of all phenotypes, and then reduce our models
169 by combining only the statistically significant individual phenotypes into a multi-variable
170 model. We further remove any phenotype that loses significance in the multi-variable model,
171 assuming that it is correlated with a more impactful phenotype. From this point, all mentions
172 of significance are obtained from the GAMM analyses with p-values < 0.01 based on Wald-
173 type tests as described in[31,32], unless otherwise stated.
174

175 ## Revealing multi-trait adaptation on a cross-patient scale

176 AA predicted six distinctive archetypes sufficient to describe each isolate within the
177 evolutionary landscape of 5 continuous traits as shown in Figure 3A. We use only growth rate

178 in ASM due to its correlation with growth rate in LB (Figure 3D). The simplex plot of Figure 3C
179 highlights the standout features of each archetype by annotating according to the highest or
180 lowest values for each phenotype across all archetype trait profiles (Figure 3B). This simplex
181 key illustrates that two archetypes resembled naïve and un-evolved isolates with fast growth,
182 antibiotic susceptibility, and low adherence (Archetype A3 and A5), while two others
183 accounted for slow-growing evolved archetypes (A2 and A6), in accordance with the accepted
184 paradigm[10,24]. A substantial portion of isolates in our study resemble the naïve archetypes
185 more closely than the evolved archetypes as indicated by their localization in the simplex plot
186 (Figure 3C, most isolates cluster on the left near the naïve archetypes). This aligns with the
187 infection stage of the patients included in this study. Importantly, we also find two regions in
188 the simplex visualization which represent different focal points of adaptation: 1) an increase
189 in adherence (A2 and A4) and 2) ciprofloxacin resistance (A1 and A6).
190
191 We also built a GAMM for each of our six continuous phenotypes to identify whether any of
192 the other traits and time influenced it significantly across our patient cohort (Figure 3D).
193 When evaluating adaptation of the specific phenotypes, we found that the colonization time
194 had a significant impact on both growth rate and sensitivity to ciprofloxacin but did not
195 significantly influence sensitivity to aztreonam (Figure 3C, Figure 4A and 4B), which is a
196 reflection of the regular administration of ciprofloxacin but not aztreonam to our patients[33].
197

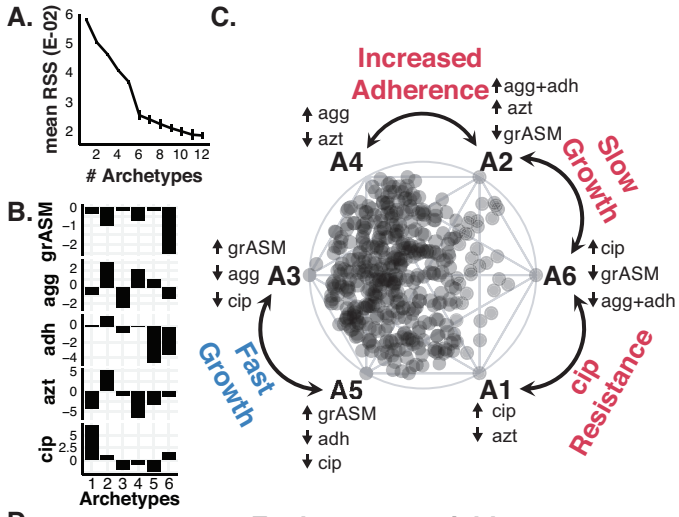

D. Predicted variable — Explanatory variables

	ColT	grASM	grLB	azt	adh	agg	prot	mut
grASM	0.0062	-	2.0E-16	-	NA	6.8E-15	-	-
grLB	0.0003	2.0E-16	-	NA	-	-	-	-
azt	-	-	-	-	NA	-	-	0.0003
cip	2.7E-07	-	-	0.0072	-	-	-	0.0122
adh	-	NA	0.0063	NA	-	0.0001	-	-
agg	-	3.0E-08	-	-	0.0053	-	2.3E-05	-

*cip and mucoid as explanatory variables did not show any significant impact on any of the predictors.

Figure 3. *AA and GAMM models.* We present a summary of the models underpinning our study of pathogen adaptation. **(A)** Screeplot showing the average residual sum of squares (RSS) for 25 iterations of each fit of a given number of archetypes. The "elbow" of the plot indicates that six archetypes are sufficient to model our dataset. **(B)** Characteristic trait profiles describing the 5 distinct phenotype levels that each of our 6 archetypes represents. We use the following abbreviations to represent our normalized data: grASM – growth rate in ASM, agg – Aggregation, adh – Adhesion, azt – aztreonam susceptibility, cip – ciprofloxacin susceptibility. **(C)** Simplex plot of the AA showing the six archetypes (A1-A6) sorted by their characteristic growth rate (A3 and A5 vs A2 and A6), decreased sensitivity towards ciprofloxacin (A1 and A6), and increased aggregation and adhesion (A2 and A4). All further simplex visualizations are also sorted accordingly and can be interpreted using this key, which is annotated with the extreme phenotype values for each archetype. The complete analysis can be found in Supplementary material 1. **(D)** P-values for GAMM models with multiple explanatory variables (columns) for the six predictor variables (rows), after model reduction. P-values are only shown for explanatory variables that showed a significant (p-value<0.01) impact on the predictor in question. The complete analysis can be found in Supplementary material 2.

Phenotypic trends contrast with CF paradigms

An important distinction between AA and GAMMs is that many isolates clearly cluster in AA according to phenotypes whose adaptation is not significantly influenced by time of colonization as shown by GAMMs. This contrast shows the importance of combining these approaches to understand our data. As an example, both adhesion and aggregation do not correlate with colonization time for this population of young patients, though we see selection for adherence in a few specific patients via AA. That this is not a major trend in our data is surprising when we consider that a biofilm lifestyle is expected to be beneficial to persistence in chronically infected patients[4,34–36]. Furthermore, the biofilm-related metric of

209 mucoidity does not significantly correlate with any other measured phenotype, despite its
210 use as an important biomarker of chronic infection in the Copenhagen CF Centre[37]. We
211 hypothesize that the rate of adaptation and relative benefit of this phenotype may vary
212 significantly and be sensitive to temporal stresses such as antibiotic treatment. In support of
213 our findings, others have recently shown that the longitudinal relationship between
214 mucoidity and a clinical diagnosis of chronic infection is not as direct as previously expected[38].
215 Together, these results prompt further reassessment of common assumptions regarding the
216 evolutionary objectives of *P. aeruginosa* in CF infections.
217

218 ## Initial adaptation happens within 3 years of colonization

219 We find that the routes to successful persistence and a transition to chronic infection are
220 initiated early in infection[16,39]. The GAMMs indicate that a substantial change occurs in both
221 growth rate and ciprofloxacin susceptibility during the first 2-3 years (5256 - 7884 bacterial
222 generations[23]) of colonization as shown by the slopes in this period (Figure 4A-B). Using AA,
223 we also see a substantial shift from naïve towards evolved archetypes as shown by the broad
224 distribution of isolates reaching the outer simplex boundaries by year 3 (Figure 4C), further
225 confirming the rapid adaptation shown by the GAMMs. While the first isolate of each patient
226 in our collection may not represent the true start of adaptation given sampling limitations,
227 the window of rapid adaptation is still likely substantially contracted compared to the
228 previous estimate of within 42,000 generations[9]. In fact, our data resembles the rate of fitness
229 improvement found in the laboratory evolution study of *Escherichia coli* that showed change
230 within the first 5,000-10,000 generations[6,7].
231

232 Interestingly, the four hypermutator isolates arising in the early adaptation window do not
233 alone define the AA boundary, indicating that the acquisition of a high number of mutations
234 does not explain all extreme phenotypes (Figure 4D, full dataset in Figure S1). To further
235 evaluate parallels between phenotypic and genetic adaptation, we investigated the
236 accumulation of nonsynonymous mutations in coordination with archetypal relationships
237 (Figure 4D-E). We used the isolates representing the first *P. aeruginosa* culture from a patient
238 as the reference point for identification of accumulating mutations. We observed that most
239 of the first isolates with 0-30 mutations aligned with naïve archetypes, and 2-3-year-old

240 isolates with 9-48 mutations extended to the outer boundaries of adaptation (A2, A6, and A1)
241 (Figure 4C-D). We also observed the persistence of WT-like genotypes with few mutations
242 alongside evolved genotypes (Figure 4D). Thus, we find discordant molecular and phenotypic
243 adaptation from a multi-trait perspective.
244

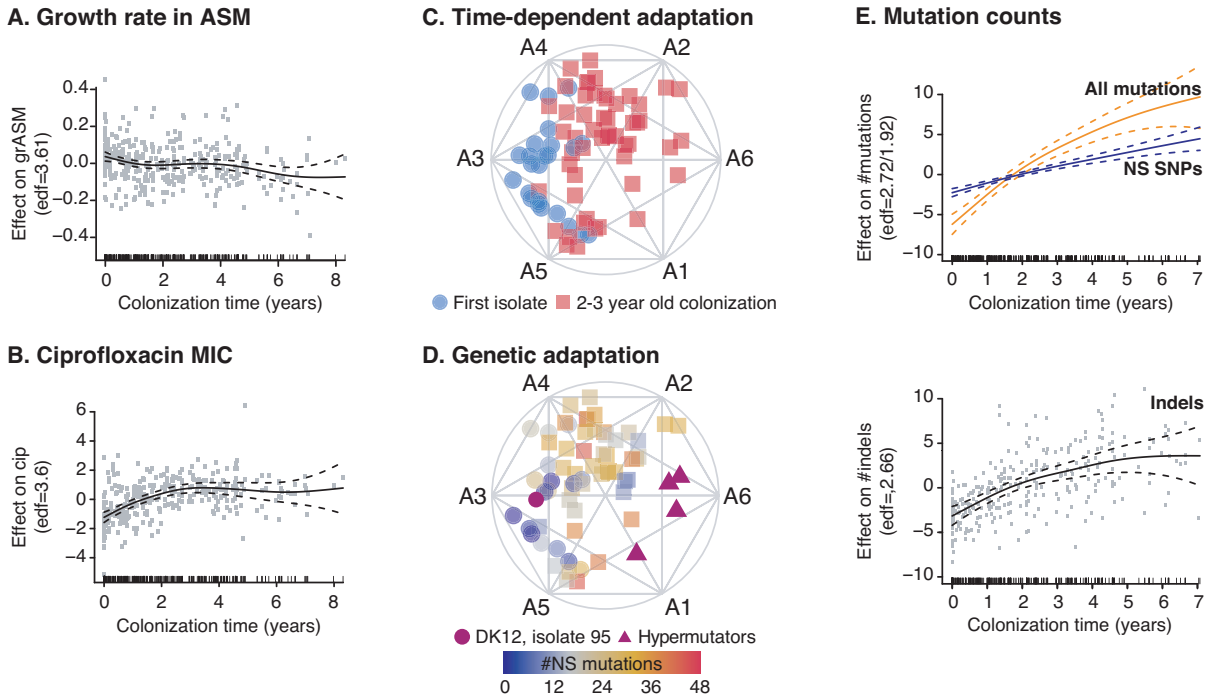

245

Figure 4. *Rapid early adaptation.* We present specific GAMM and AA models to illustrate the rapid adaptation of growth rate and ciprofloxacin over time and contrast these patterns with genetic adaptation via the accumulation of nonsynonymous mutations. Here, we use GAMMs to illustrate the significant impact of the explanatory variable colonization time on **(A)** growth rate in ASM, **(B)** ciprofloxacin sensitivity in ASM, **(E)** the accumulation of all mutations (orange) and nonsynonymous SNPs (blue) and indels (insertions and deletions). We use simplex visualizations of AA to show **(C)** "naïve" trait alignment of the first isolate of the twenty patients where we have analyzed the first *P. aeruginosa* isolate ever cultured at the CF clinic (blue circles) in contrast to "evolved" isolates that have been cultured at year 2-3 of colonization (red squares, all patients of the dataset). We contrast this trait-based ordination with **(D)** genetic adaptation, shown by a color overlay of the number of nonsynonymous mutations present in each isolate. Isolate 95 (purple circle) of the DK12 clone type has a very high number of mutations (>100) because one isolate in that lineage (isolate 96) is very different from the remaining 11 isolates. For the GAMM analysis shown in Figure 4E, we filtered out the mutations from the errant DK12 96 single isolate that affected the whole lineage. Hypermutators are marked by purple triangles. **(A/B/E notation)** GAMMs are illustrated by solid smoothed trendlines, dashed two standard error bounds, and gray points as residuals. Y-axes are labelled by the predictor variable on which the effect of colonization time of the clone type ("ColT") has been estimated as well as the estimated degrees of freedom (edf) (for the E upper panel the edf is ordered as all mutations/NS SNPs). Residuals have not been plotted in the upper panel of **(E)** for clarity reasons. X-axes are the ColT in years and patients are included as random smooths together with ColT. A rug plot is also visible on the x-axis to indicate the density of observations over time.

246

247 When analyzing the entire dataset using GAMMs, we found a significant, near-linear
248 relationship between colonization time and the number of nonsynonymous SNPs, but

249 accumulation of all nonsynonymous mutations appears logarithmic with accumulation
250 slowing after 2 years (Figure 4E). This behavior resembles that of the laboratory evolution of
251 *E. coli* (propagated for more than 60,000 generations)[40], though accumulation may slow
252 sooner in the CF lung. When we plot accumulation of indels alone, we see the likely driver of
253 the logarithmic trend. When combined with the discordance found by AA, these findings
254 support the theory that select beneficial mutations (for example, a highly impactful indel) can
255 alone induce important phenotypic changes that improve fitness[41]. However, the likelihood
256 of beneficial mutations presumably decreases over time as theorized previously[42] and other
257 methods of adaptation also contribute, such as acclimation to the CF lung environment via
258 gene expression changes[43,44].
259

260 ## Multi-trait analysis enables complex genotype-phenotype associations

261 The obscuring of genotype-phenotype links via polygenic effects and the possible pleiotropic
262 effects of single mutations is difficult to resolve, especially when working with complex traits.
263 However, we have a unique multi-dimensional perspective from which to map genotype-
264 phenotype relationships. We previously identified 52 "pathoadaptive genes" - genes mutated
265 more often than expected from genetic drift and thus assumed to confer an adaptive
266 advantage during infection[16,45]. By overlaying nonsynonymous mutations on AA simplex plots,
267 we evaluated the impact of mutation of the following pathoadaptive genes: 1) *mexZ* (the most
268 frequently mutated gene) and other repressors of drug efflux pumps (*nfxB* and *nalD*), 2)
269 mucoidity regulators *mucA* and *algU* and the hypothesized infection-state switching
270 *retS*/*gacAS*/*rsmA* regulatory pathway previously examined from a genetic adaptation
271 perspective[16,46], and 3) ciprofloxacin resistance genes *gyrA* and *gyrB*[47–49]. Isolates with *mexZ*
272 mutations are broadly distributed by AA, so we analyzed *mexZ* mutants in combination with
273 other pump repressor gene mutations. Even double-mutant isolates (grouped by efflux pump
274 associations) showed diverse phenotypes via AA, though we noted a unique distribution of
275 the many isolates impacted by a mutation in *nfxB* (Figure S3, Figure 5B). We saw no obvious
276 spatial correlations with mutations linked to mucoidity regulation via AA (Figure S2),
277 paralleling mucoidity's lack of significance in our GAMM analyses. However, the isolate
278 distributions of *retS/gacAS/rsmA* and *gyrA/B* mutants were striking in their spatial
279 segregation (Figure 5A-B).

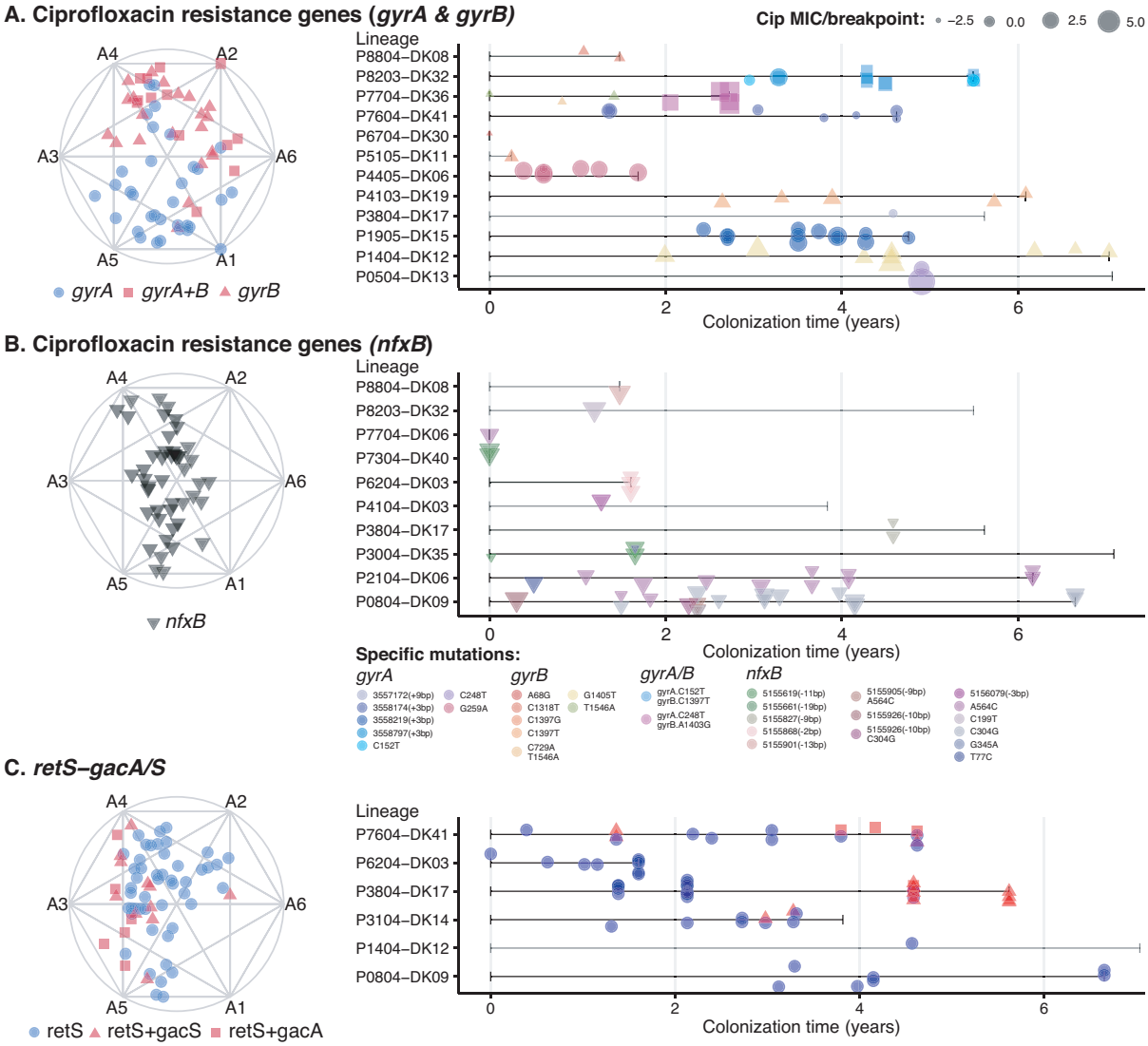

Figure 5. *Mechanistic links between phenotypic changes and mutations in ciprofloxacin resistance genes and the retS/gacAS/rsmA system.* We use AA to illustrate phenotypic separation by isolates affected by distinct mutations in ciprofloxacin resistance genes *gyrA*, *gyrB*, and *nfxB* and the *retS/gacAS/rsmA* regulatory system. **(A-B, left panel)** As visualized by AA simplex plots, the diversity of trait profiles associated with isolates with mutations in DNA gyrase (*gyrA/B*) is in stark contrast to the constrained band of *nfxB*-mutated isolates. Mutations in DNA gyrase and *nfxB* do not co-occur in the same isolate but co-occur in different isolates of 2 lineages (patient P8804, genotype DK08 and patient P8203, genotype DK32). The differences in time of appearance during the colonization period and persistence of *gyrA*/*B* mutant isolates versus *nfxB* mutant isolates is shown in the lineage timelines plotted in the right column for *gyrA/B* **(A, right panel)** versus *nfxB* **(B, right panel)**. Furthermore, *gyrB*-mutated isolates cluster more closely with A2 and A4 than *gyrA* mutated isolates, indicating a potential association with adhesion; GAMMs predicts that *gyrB* mutation has a significant impact on adhesion (GAMM, p-value << 0.01). **(C, left panel)** Mutations in the *retS/gacAS/rsmA* system shows a clear phenotypic change when *retS* is mutated alone (blue circles) or in combination with *gacA* or *gacS* (red squares and circles). The associated lineage plot **(C, right panel)** shows the appearance of double mutations (*retS* + *gacA/S*) after a colonization period by *retS* mutated isolates in three patient lineages. **(A/B/C – lineage plot notation)** Lineage length is based on the span of time for which we have collected isolates and is indicated by gray bracketed lines, with only isolates affected by a mutation of interest plotted using shape to indicate mutation type. Symbol color indicates the specific mutation location in the affected gene and **(A/B only)** symbol size indicates the level of resistance to ciprofloxacin. Multiple isolates may be collected at the same sampling date based on differences in colony morphology or collected from different sinuses at sinus surgery, which explains the vertical overlap of isolates for some lineages.

282 *Differential evolutionary potential via ciprofloxacin resistance mechanisms*

283 The primary drivers of ciprofloxacin resistance in *P. aeruginosa* are theorized to be mutations
284 in drug efflux pump repressor *nfxB* and the gyrase subunits *gyrA* and *gyrB* of the DNA
285 replication system[47–49]. We would therefore expect isolates with mutations in these genes to
286 cluster around archetypes A1 and A6 characterized by high ciprofloxacin minimal inhibitory
287 concentrations (MICs) (Figure 3C). However, AA illustrates a broad distribution of *gyrA/B*
288 mutants among archetypes, and a contrasting narrow distribution of *nfxB* mutants (Figure 5A-
289 B, left panel). In association, we see a range of ciprofloxacin resistance levels associated with
290 affected isolates both across and within patient lineages, and no dominant
291 mutations/mutated regions repeating across lineages (Figure 5A-B, right panel). The
292 incidence of resistance due to these distinct mechanisms was equal at 78% of affected isolates
293 (54 out of 69 resistant gyrase mutants vs 37 out of 47 resistant *nfxB* mutants based on the
294 European Committee on Antimicrobial Susceptibility Testing (EUCAST) breakpoint). However,
295 the persistence of these respective mutations in affected lineages was dissimilar. Generally,
296 *nfxB* mutation occurred earlier in lineage evolution and persisted in fewer lineages compared
297 to *gyrA/B* mutations. This likely contributes to *nfxB*'s distinctive band-like distribution via AA
298 which suggests an evolutionary restriction associated with sustaining the mutation.

299

300 Interestingly, we noted that isolates with a *gyrB* mutation (22 isolates alone or 14 in concert
301 with *gyrA* mutation) are concentrated closer to "biofilm-linked" archetypes A2 and A4 than
302 isolates with only a *gyrA* mutation (33 isolates). To our knowledge, there is no direct
303 relationship between *gyrB* and the capability to adhere[49]. This positive association of *gyrB* on
304 adhesion was confirmed by GAMM, but when we moved the two SNPs affecting the most
305 isolates in both *gyrA* and *gyrB* (2 lineages each, Figure S4) into lab strain *P. aeruginosa*
306 PAO1, we did not find the same association (Figure S5-6) (p-values > 0.05, ANOVA with Tukey
307 correction, $F(4,10)=0.233$). We then looked for co-occurring mutations in biofilm-linked genes
308 in the *gyrB*-mutated lineages; for all but one lineage, there was no obvious explanation for
309 increased adhesion. Ultimately, this association underlines the impact that genetic
310 background and the multi-genetic signature of biofilm regulation can have on the
311 identification of links between genotype and phenotype[50].

312

313 *Infection trajectory reversal via a regulatory switch*

314 The functional model of the *retS*/*gacA*/*gacS*/*rsmA* regulatory system is theorized to be a
315 bimodal switch between acute and chronic infection phenotypes[46,51]. Posttranscriptional
316 regulator *rsmA* activates an acute infection phenotype characterized by planktonic growth
317 and inhibits a non-motile biofilm lifestyle. *retS* mutants are preserved in many lineages
318 because they repress *rsmA* via the *gacA/S* two-component system, promoting a chronic
319 infection phenotype. However, our previous genetic analysis[16] unexpectedly showed that
320 multiple evolving lineages gained a subsequent mutation in *gacA*/*S* that often appeared years
321 after the *retS* mutation. Despite the complexity of this regulatory system, we show a clear
322 phenotypic separation between clinical isolates that are *retS* mutants versus *retS+gacA*/*S*
323 mutants via our AA model (Figure 5C, left panel). In this study, three of six patients with
324 nonsynonymous mutations in this system have isolates which are *retS+gacA*/*S* double
325 mutants (Figure 5C, right panel). While *retS* mutants resemble the evolved archetypes (A1 –
326 2 and A6), all but one double mutant clusters around the naïve archetypes (A3 – A5).
327 According to patient-specific trajectories, this reversion happens after an initial migration
328 towards evolved archetypes. Because of the limited isolates and patients affected, we did not
329 follow up with additional GAMM analyses of the effect of these mutations on different
330 phenotypes.
331
332 This unexpected phenotypic reversion to an "acute infection state" does not easily reconcile
333 with theories about persistence via convergence towards a "chronic phenotype". However,
334 over time some patients are colonized by new clone types and/or other pathogens; this could
335 require re-establishment of a colonization mid-infection and thus induce the population to
336 revert towards an acute infection state where fast growth and motility improve its ability to
337 compete.
338

339 ## Infections persist via distinct routes of adaptation

340 Given the above insights from lineage-based analysis, we further investigate lineage
341 influences by mapping patient-specific adaptive trajectories. We find 3 overarching modes of
342 evolution that *P. aeruginosa* can utilize to persist successfully in individual patients: 1)
343 convergent evolution, 2) directed diversity or 3) general diversity. Figure 6A-D shows
344 examples of adapting lineages employing these modes. We see rapid convergent evolution

345 towards an endpoint of ciprofloxacin resistance in patient P5304 (Figure 6A). Diverse isolates
346 appear to move in the same general direction of increased adhesion and aggregation in
347 patient P4104 (Figure 6B), which we term "directed diversity", while no directionality is
348 apparent in the diverse isolates of the trajectory of patient P0804 (Figure 6C), which we term
349 "general diversity". In the complex trajectory of patient P1404 (Figure 6D), the genotypic
350 distinction of the young isolate near A4 indicates that the persisting sublineage initiates with
351 the isolate near A3, after which it gains a *gyrB* mutation guiding the trajectory towards
352 ciprofloxacin resistant A1. This mutation is retained during the subsequent shift towards A2,
353 characterized by increased adherence and decreased sensitivity to aztreonam. These results
354 illustrate the diverse adaptive trajectories followed by *P. aeruginosa* in our patient cohort,
355 which connect distinct start and endpoints of adaptation yet enable years of persistence.
356

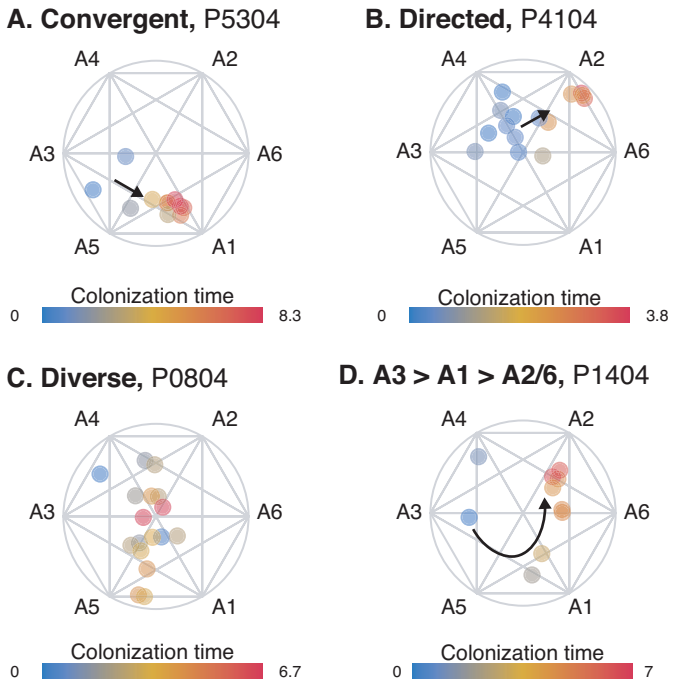

357

Figure 6. *Evolutionary trajectories guided by different adaptation needs.* We present four different trajectories showing modes of evolution found in multiple patients: **(A)** Convergent evolution driven primarily by changes of a single phenotypic trait (decreased ciprofloxacin sensitivity). **(B)** Directed diversity with early/naïve isolates showing a population moving in a broad and diverse plane from naïve archetypes towards evolved archetypes. **(C)** General diversity where the population has no clear evolutionary trajectory. **(D)** A special case of convergent evolution with one outlier isolate (isolate 96 of DK12) but an otherwise clear trajectory first towards ciprofloxacin resistance and afterwards a gain in adhesive capabilities.

358

359 Here, we draw specific examples from patients with high sampling resolution and at least 3
360 years of infection within our cohort, but to capture the full spectrum of evolutionary modes
361 will require more uniform cross-cohort sampling that also addresses population dynamics as

362 well as the inclusion of more patients. With these expansions, we theorize that distinctive
363 evolutionary trajectories will correlate with infection persistence and patient outcomes.
364

365 DISCUSSION

366 Complex mutation patterns are an inherent byproduct of evolution and result in equally
367 complex adaptive trajectories that lead to persistence. Phenotype represents the cumulative
368 systems-level impacts of these mutation patterns. We therefore emphasize the value of
369 classical phenotype-based investigations as a highly relevant complement to genomics
370 approaches. By integrating these perspectives via our statistical modeling framework, it is
371 possible to identify consistent pan-cohort trends while illuminating complex patient-specific
372 patterns and their genetic drivers. This approach could also be valuable in assessing evolution-
373 based scenarios such as interpretation of laboratory evolution experiments, investigations of
374 long-term microbiome fluctuations and other studies of evolving clonal populations.
375
376 Our study identifies rapid phenotypic adaptation of isolates within the first few years of
377 colonization by both mutational accumulation and acclimation as indicated by the
378 discordance between genotypic and phenotypic adaptation. This resembles the findings from
379 the long-term laboratory evolution of *E. coli*[40]. While specific traits show cross-patient
380 convergence (growth rate and ciprofloxacin resistance), we highlight remarkable diversity
381 both within and across patients. In addition to convergent and directed evolution, we thus
382 emphasize the maintenance of general diversity as a useful evolutionary mode of persistence
383 as supported by prior observations of resilience in diverse populations[52–54]. Among our
384 patient-specific trajectories, we also find varying routes within these categories of evolution
385 that are used by different patient lineages to achieve successful persistence. These important
386 evolutionary findings can further be translated to the clinic. Although early aggressive
387 antibiotic therapy has been shown to substantially delay the transition to chronic infection[33],
388 we provide a valuable estimate of this narrow window based on analysis at high temporal
389 resolution. Furthermore, we provide a quantitative approach to monitoring infection state
390 via patient-specific trajectories which can offer important insights into bacterial response to
391 treatment.
392

393 Given that individual mutations may have pleiotropic effects and obscure genetic signatures
394 as they accumulate over time[19], our study underlines the necessity of a multi-trait
395 perspective. Our genotype-phenotype associations support the theory that specific mutations
396 confer unique evolutionary restrictions to adaptive trajectories; these restrictions impact the
397 fixation of other mutations or adaptation of other traits, but genetic background and host-
398 specific evolutionary pressures influence the type and degree of restriction[8]. By mapping
399 phenotypic trajectories, we can identify both genetic mechanisms that regulate these
400 highways and complex traits that signal the impact of treatment on individual infections. In
401 the future, we see particular promise in incorporating records of patient treatment and
402 response to our assessment of adaptive trajectories to further guide clinicians and advance
403 precision medicine in clinical microbiology.
404

405 ACKNOWLEDGMENTS

406 HKJ was supported by The Novo Nordisk Foundation as a clinical research stipend
407 (NNF12OC1015920), by Rigshospitalets Rammebevilling 2015-17 (R88-A3537), by
408 Lundbeckfonden (R167-2013-15229), by Novo Nordisk Fonden (NNF15OC0017444), by
409 RegionH Rammebevilling (R144-A5287) and by Independent Research Fund Denmark /
410 Technology and Production Sciences (FTP-4183-00051). JAB was funded by a postdoctoral
411 fellowship from the Whitaker Foundation. We thank Katja Bloksted, Ulla Rydahl Johansen,
412 Helle Nordbjerg Andersen, Sarah Buhr Bendixen, Camilla Thranow, Pia Poss, Bonnie Horsted
413 Erichsen, Rakel Schiøtt and Mette Pedersen for excellent technical assistance. We also thank
414 Prof. Anders Stockmarr, Prof. Nina Jakobsen and Prof. Morten Mørup (DTU Compute) and Dr.
415 Kevin D'Auria (Counsyl) for helpful discussions.
416

417 AUTHOR CONTRIBUTIONS

418 SM and HKJ jointly supervised the study. JAH, SM, and HKJ conceived and designed the
419 experiments. JAH performed all phenotypic screening with assistance from AL. REP
420 performed the genetic engineering of isolate mutations. JAB and LMS conceived and
421 performed all computational analysis and wrote the manuscript. JAH, SM and HKJ helped
422 write the manuscript and provided revisions.

423

424 DATA AND SOFTWARE AVAILABILITY

425 We provide our complete phenotype dataset in raw form as a supplemental spreadsheet and
426 include a visualization and summary statistics of normalized data in Figure 2. Data
427 normalization, processing and construction of all models was performed in R as described
428 above and all essential code for reproduction of these steps is provided in R Markdown format
429 in supplemental files 1-2. These files also include code for replicating the model visualizations
430 of Figure 3A-D and Figure 4A-C, E. Code to reproduce various secondary analysis figures is
431 available on request. All genomic information is publicly available as described in [16].

432

433 DECLARATION OF INTERESTS

434 The authors declare no competing financial interests.

435

436 REFERENCES

437 1. Flores-Mireles, A. L., Walker, J. N., Caparon, M. & Hultgren, S. J. Urinary tract
438 infections: Epidemiology, mechanisms of infection and treatment options. *Nat. Rev.*
439 *Microbiol.* **13,** 269–284 (2015).
440 2. Rau, M. H. *et al.* Early adaptive developments of *Pseudomonas aeruginosa* after the
441 transition from life in the environment to persistent colonization in the airways of
442 human cystic fibrosis hosts. *Environ. Microbiol.* **12,** 1643–1658 (2010).
443 3. Lieberman, T. D. *et al.* Genetic variation of a bacterial pathogen within individuals
444 with cystic fibrosis provides a record of selective pressures. *Nat. Genet.* **46,** 82–7
445 (2014).
446 4. Cohen-Cymberknoh, M., Shoseyov, D. & Kerem, E. Managing cystic fibrosis: Strategies
447 that increase life expectancy and improve quality of life. *Am. J. Respir. Crit. Care Med.*
448 **183,** 1463–1471 (2011).
449 5. Cooper, T. F. & Lenski, R. E. Experimental evolution with E. coli in diverse resource
450 environments. I. Fluctuating environments promote divergence of replicate
451 populations. *BMC Evol. Biol.* **10,** 11 (2010).

452 6. Woods, R. J. *et al.* Second-order selection for evolvability in a large Escherichia coli
453 population. *Science* **331,** 1433–6 (2011).
454 7. Barrick, J. E. *et al.* Genome evolution and adaptation in a long-term experiment with
455 Escherichia coli. *Nature* **461,** 1243–1247 (2009).
456 8. Leon, D., D'Alton, S., Quandt, E. M. & Barrick, J. E. An evolutionary innovation is
457 contingent on maintaining adaptive potential until competition subsides. *PLoS Genet.*
458 **14,** 249110 (2018).
459 9. Yang, L. *et al.* Evolutionary dynamics of bacteria in a human host environment. *Proc.*
460 *Natl. Acad. Sci. U. S. A.* **108,** 7481–6 (2011).
461 10. Winstanley, C., O'Brien, S. & Brockhurst, M. A. Pseudomonas aeruginosa Evolutionary
462 Adaptation and Diversification in Cystic Fibrosis Chronic Lung Infections. *Trends*
463 *Microbiol.* **24,** 327–337 (2016).
464 11. Markussen, T. *et al.* Environmental heterogeneity drives within-host diversification
465 and evolution of Pseudomonas aeruginosa. *MBio* **5,** e01592-14 (2014).
466 12. Jorth, P. *et al.* Regional Isolation Drives Bacterial Diversification within Cystic Fibrosis
467 Lungs. *Cell Host Microbe* **18,** 307–19 (2015).
468 13. Imamovic, L. *et al.* Drug-Driven Phenotypic Convergence Supports Rational Treatment
469 Strategies of Chronic Infections. *Cell* **172,** 121–134.e14 (2018).
470 14. Marvig, R. L., Johansen, H. K., Molin, S. & Jelsbak, L. Genome Analysis of a
471 Transmissible Lineage of Pseudomonas aeruginosa Reveals Pathoadaptive Mutations
472 and Distinct Evolutionary Paths of Hypermutators. *PLoS Genet.* **9,** e1003741 (2013).
473 15. Smith, E. E. *et al.* Genetic adaptation by Pseudomonas aeruginosa to the airways of
474 cystic fibrosis patients. *Proc. Natl. Acad. Sci. U. S. A.* **103,** 8487–92 (2006).
475 16. Marvig, R. L., Sommer, L. M., Molin, S. & Johansen, H. K. Convergent evolution and
476 adaptation of Pseudomonas aeruginosa within patients with cystic fibrosis. *Nat.*
477 *Genet.* **47,** (2015).
478 17. Silva, I. N. *et al.* Long-Term Evolution of *Burkholderia multivorans* during a Chronic
479 Cystic Fibrosis Infection Reveals Shifting Forces of Selection. *mSystems* **1,** e00029-16
480 (2016).
481 18. Sommer, L. M. *et al.* Bacterial evolution in PCD and CF patients follows the same
482 mutational steps. *Sci. Rep.* **6,** 28732 (2016).
483 19. Boyle, E. A., Li, Y. I. & Pritchard, J. K. An Expanded View of Complex Traits: From

484 Polygenic to Omnigenic. *Cell* **169,** 1177–1186 (2017).
485 20. Deatherage, D. E., Kepner, J. L., Bennett, A. F., Lenski, R. E. & Barrick, J. E. Specificity
486 of genome evolution in experimental populations of Escherichia coli evolved at
487 different temperatures. *Proc. Natl. Acad. Sci. U. S. A.* **114,** E1904–E1912 (2017).
488 21. Jansson, J. K. & Hofmockel, K. S. The soil microbiome — from metagenomics to
489 metaphenomics. *Curr. Opin. Microbiol.* **43,** 162–168 (2018).
490 22. Sommer, L. M. *et al.* Is genotyping of single isolates sufficient for population structure
491 analysis of Pseudomonas aeruginosa in cystic fibrosis airways? *BMC Genomics* **17,**
492 (2016).
493 23. Yang, L. *et al.* In situ growth rates and biofilm development of Pseudomonas
494 aeruginosa populations in chronic lung infections. *J. Bacteriol.* **190,** 2767–76 (2008).
495 24. Moradali, M. F., Ghods, S. & Rehm, B. H. A. Pseudomonas aeruginosa Lifestyle: A
496 Paradigm for Adaptation, Survival, and Persistence. *Front. Cell. Infect. Microbiol.* **7,**
497 393389–39 (2017).
498 25. Furukawa, S., Kuchma, S. L. & O'Toole, G. A. Keeping their options open: acute versus
499 persistent infections. *J. Bacteriol.* **188,** 1211–7 (2006).
500 26. Andersen, S. B., Marvig, R. L., Molin, S., Krogh Johansen, H. & Griffin, A. S. Long-term
501 social dynamics drive loss of function in pathogenic bacteria. *Proc. Natl. Acad. Sci. U.*
502 *S. A.* **112,** 10756–61 (2015).
503 27. Thøgersen, J., Mørup, M., Damkiær, S., Molin, S. & Jelsbak, L. Archetypal analysis of
504 diverse Pseudomonas aeruginosa transcriptomes reveals adaptation in cystic fibrosis
505 airways. *BMC Bioinformatics* **14,** 279 (2013).
506 28. Sheftel, H., Szekely, P., Mayo, A., Sella, G. & Alon, U. Evolutionary trade-offs and the
507 structure of polymorphisms. *Philos. Trans. R. Soc. Lond. B. Biol. Sci.* **373,** 20170105
508 (2018).
509 29. Mørup, M. & Hansen, L. K. Archetypal analysis for machine learning and data mining.
510 *Neurocomputing* **80,** 54–63 (2012).
511 30. Seth, S. & Eugster, M. J. A. Probabilistic archetypal analysis. *Mach. Learn.* **102,** 85–113
512 (2016).
513 31. Wood, S. N. *Generalized additive models : an introduction with R*. (CRC Press, 2006).
514 32. Wood, S. N. On p-values for smooth components of an extended generalized additive
515 model. *Biometrika* **100,** 221–228 (2013).

516 33. Hansen, C. R., Pressler, T. & Høiby, N. Early aggressive eradication therapy for
517 intermittent Pseudomonas aeruginosa airway colonization in cystic fibrosis patients:
518 15 years experience. *J. Cyst. Fibros.* **7,** 523–30 (2008).
519 34. Høiby, N. Understanding bacterial biofilms in patients with cystic fibrosis: current and
520 innovative approaches to potential therapies. *J. Cyst. Fibros.* **1,** 249–254 (2002).
521 35. Bjarnsholt, T. *et al. Pseudomonas aeruginosa* biofilms in the respiratory tract of cystic
522 fibrosis patients. *Pediatr. Pulmonol.* **44,** 547–558 (2009).
523 36. Pressler, T. *et al.* Chronic Pseudomonas aeruginosa infection definition: EuroCareCF
524 Working Group report. *J. Cyst. Fibros.* **10,** S75–S78 (2011).
525 37. Pedersen, S. S., Høiby, N., Espersen, F. & Koch, C. Role of alginate in infection with
526 mucoid Pseudomonas aeruginosa in cystic fibrosis. *Thorax* **47,** 6–13 (1992).
527 38. Heltshe, S. L. *et al.* Longitudinal development of initial, chronic and mucoid
528 Pseudomonas aeruginosa infection in young children with cystic fibrosis. *J. Cyst.*
529 *Fibros.* (2017). doi:10.1016/j.jcf.2017.10.008
530 39. Hansen, S. K. *et al.* Evolution and diversification of Pseudomonas aeruginosa in the
531 paranasal sinuses of cystic fibrosis children have implications for chronic lung
532 infection. *ISME J.* **6,** 31–45 (2012).
533 40. Good, B. H., McDonald, M. J., Barrick, J. E., Lenski, R. E. & Desai, M. M. The dynamics
534 of molecular evolution over 60,000 generations. *Nature* **551,** 45–50 (2017).
535 41. Solovieff, N., Cotsapas, C., Lee, P. H., Purcell, S. M. & Smoller, J. W. Pleiotropy in
536 complex traits: challenges and strategies. *Nat. Rev. Genet.* **14,** 483–495 (2013).
537 42. Desai, M. M. & Fisher, D. S. Beneficial mutation selection balance and the effect of
538 linkage on positive selection. *Genetics* **176,** 1759–98 (2007).
539 43. Dötsch, A. *et al.* The Pseudomonas aeruginosa Transcriptional Landscape Is Shaped by
540 Environmental Heterogeneity and Genetic Variation. *MBio* **6,** e00749 (2015).
541 44. Rossi, E., Falcone, M., Molin, S. & Johansen, H. K. High-resolution in situ
542 transcriptomics of Pseudomonas aeruginosa unveils genotype independent patho-
543 phenotypes in cystic fibrosis lungs. *Submitted* (2018).
544 45. Sokurenko, E. V *et al.* Pathoadaptive mutations: gene loss and variation in bacterial
545 pathogens. *Trends Microbiol.* **7,** 191–5 (1999).
546 46. Goodman, A. L. *et al.* A Signaling Network Reciprocally Regulates Genes Associated
547 with Acute Infection and Chronic Persistence in Pseudomonas aeruginosa. *Dev. Cell* **7,**

548 745–754 (2004).
549 47. Robillard, N. J. & Scarpa, A. L. Genetic and physiological characterization of
550 ciprofloxacin resistance in Pseudomonas aeruginosa PAO. *Antimicrob. Agents*
551 *Chemother.* **32,** 535–9 (1988).
552 48. Nakamura, S., Nakamura, M., Kojima, T. & Yoshida, H. gyrA and gyrB mutations in
553 quinolone-resistant strains of Escherichia coli. *Antimicrob. Agents Chemother.* **33,**
554 254–5 (1989).
555 49. Kugelberg, E., Löfmark, S., Wretlind, B. & Andersson, D. I. Reduction of the fitness
556 burden of quinolone resistance in Pseudomonas aeruginosa. *J. Antimicrob.*
557 *Chemother.* **55,** 22–30 (2005).
558 50. Wolska, K. I., Grudniak, A. M., Rudnicka, Z. & Markowska, K. Genetic control of
559 bacterial biofilms. *J. Appl. Genet.* **57,** 225–38 (2016).
560 51. Ventre, I. *et al.* Multiple sensors control reciprocal expression of Pseudomonas
561 aeruginosa regulatory RNA and virulence genes. *Proc. Natl. Acad. Sci. U. S. A.* **103,**
562 171–6 (2006).
563 52. Wolf, D. M., Vazirani, V. V. & Arkin, A. P. Diversity in times of adversity: probabilistic
564 strategies in microbial survival games. *J. Theor. Biol.* **234,** 227–253 (2005).
565 53. KOH, K. S. *et al.* Minimal increase in genetic diversity enhances predation resistance.
566 *Mol. Ecol.* **21,** 1741–1753 (2012).
567 54. Boles, B. R., Thoendel, M. & Singh, P. K. Self-generated diversity produces '"insurance
568 effects"' in biofilm communities. *Proc. Natl. Acad. Sci.* **101,** 16630–16635 (2004).
569 55. Kirchner, S. *et al.* Use of artificial sputum medium to test antibiotic efficacy against
570 Pseudomonas aeruginosa in conditions more relevant to the cystic fibrosis lung. *J. Vis.*
571 *Exp.* e3857 (2012). doi:10.3791/3857
572 56. O'Toole, G. A. & Kolter, R. Flagellar and twitching motility are necessary for
573 Pseudomonas aeruginosa biofilm development. *Mol. Microbiol.* **30,** 295–304 (1998).
574 57. Hentzer, M. *et al.* Alginate overproduction affects Pseudomonas aeruginosa biofilm
575 structure and function. *J. Bacteriol.* **183,** 5395–401 (2001).
576 58. Ryder, C., Byrd, M. & Wozniak, D. J. Role of polysaccharides in Pseudomonas
577 aeruginosa biofilm development. *Curr. Opin. Microbiol.* **10,** 644–8 (2007).
578 59. Kragh, K. N. *et al.* Role of Multicellular Aggregates in Biofilm Formation. *MBio* **7,**
579 e00237 (2016).

580 60. Déziel, E., Comeau, Y. & Villemur, R. Initiation of biofilm formation by Pseudomonas
581 aeruginosa 57RP correlates with emergence of hyperpiliated and highly adherent
582 phenotypic variants deficient in swimming, swarming, and twitching motilities. *J.*
583 *Bacteriol.* **183,** 1195–204 (2001).
584 61. Caceres, S. M. *et al.* Enhanced in vitro formation and antibiotic resistance of
585 nonattached Pseudomonas aeruginosa aggregates through incorporation of
586 neutrophil products. *Antimicrob. Agents Chemother.* **58,** 6851–60 (2014).
587 62. Ricaurte, D. E. *et al.* A standardized workflow for surveying recombinases expands
588 bacterial genome-editing capabilities. *Microb. Biotechnol.* **11,** 176–188 (2018).
589 63. Aparicio, T., de Lorenzo, V. & Martínez-García, E. CRISPR/Cas9-Based
590 Counterselection Boosts Recombineering Efficiency in *Pseudomonas putida*.
591 *Biotechnol. J.* **13,** 1700161 (2018).
592 64. Team, R. C. R: A Language and Environment for Statistical Computing. (2017).
593 65. Wood, S. N., Pya, N. & Säfken, B. Smoothing Parameter and Model Selection for
594 General Smooth Models. *J. Am. Stat. Assoc.* **111,** 1548–1563 (2016).
595 66. Wood, S. N. Fast stable restricted maximum likelihood and marginal likelihood
596 estimation of semiparametric generalized linear models. *J. R. Stat. Soc. Ser. B*
597 *(Statistical Methodol.* **73,** 3–36 (2011).
598 67. Eugster, M. J. A. & Leisch, F. From Spider-Man to Hero - Archetypal Analysis in *R. J.*
599 *Stat. Softw.* **30,** 1–23 (2009).
600 68. Eugster, M. J. A. & Leisch, F. Weighted and robust archetypal analysis. *Comput. Stat.*
601 *Data Anal.* **55,** 1215–1225 (2011).
602 69. Seth, S. & Eugster, M. J. A. Probabilistic Archetypal Analysis. (2014).
603 70. Wickham, H. tidyverse: Easily Install and Load the 'Tidyverse'. (2017).
604 71. van Rij, J., Wieling, M., Baayen, R. H. & van Rijn, H. itsadug: Interpreting Time Series
605 and Autocorrelated Data Using GAMMs. (2017).
606 72. Arnold, J. B. ggthemes: Extra Themes, Scales and Geoms for 'ggplot2'. (2017).
607 73. Xie, Y. knitr: A General-Purpose Package for Dynamic Report Generation in R. (2017).
608 74. Zhu, H. kableExtra: Construct Complex Table with 'kable' and Pipe Syntax. (2017).
609 75. Fernandez, M., Wilson, H. F. & Barnard, A. S. Impact of distributions on the
610 archetypes and prototypes in heterogeneous nanoparticle ensembles. *Nanoscale* **9,**
611 832–843 (2017).

612 76. Johansen, H. K., Moskowitz, S. M., Ciofu, O., Pressler, T. & Høiby, N. Spread of colistin
613 resistant non-mucoid Pseudomonas aeruginosa among chronically infected Danish
614 cystic fibrosis patients. *J. Cyst. Fibros.* **7,** 391–397 (2008).
615

616 METHODS

617 The isolate collection

618 The current isolate library is comprised of 443 longitudinally collected single *P. aeruginosa*
619 isolates distributed within 52 clone types collected from 39 young CF patients treated at the
620 Copenhagen CF Centre at Rigshospitalet (median age at first *P. aeruginosa* isolate = 8.1 years,
621 range = 1.4-24.1 years, median coverage of colonization: 4.6 years, range: 0.2-10.2 years).
622 This collection is a complement to and extension of the collection previously published [16] and
623 captures the period of initial rapid adaptation[6,7,9], with 389 isolates of the previously
624 published collection included here in addition to 54 new isolates. To build a homogeneous
625 collection for our study of evolution, we excluded two patients with a sustained multi-clonal
626 infection. For the GAMM analysis, we excluded isolates belonging to clone types present in a
627 patient at two or fewer time-points, unless the two time-points were sampled more than 6
628 months apart. The isolates not included in the previous study have been clone typed as a
629 routine step at the Department of Clinical Microbiology at Rigshospitalet. This clone type
630 identification was performed as described previously[16], and the sequencing was carried out
631 as follows: DNA was purified from over-night liquid cultures of single colonies using the
632 DNEasy Blood and Tissue Kit (Qiagen), libraries were made with Nextera XT and sequenced
633 on an Illumina MiSeq using the v2 250x2 kit.
634

635 Ethics approval and consent to participate

636 The local ethics committee at the Capital Region of Denmark (Region Hovedstaden) approved
637 the use of the stored *P. aeruginosa* isolates: registration number H-4-2015-FSP.
638

639 ## Phenotypic characterizations

640 For all phenotypes except the antibiotic MIC tests, phenotypic analysis was carried out by
641 replicating from a 96 well plate pre-frozen with overnight cultures diluted with 50% glycerol
642 at a ratio of 1:1 and four technical replicates were produced for each isolate.

643

644 ### Growth rate in Luria-Bertani broth (LB) and Artificial sputum medium (ASM)[55]

645 Isolates were re-grown from frozen in 96 well plates in 150ul media (LB or ASM) and
646 incubated for 20h at 37°C with OD_{630nm} measurements every 20 min on an ELISA reader.
647 Microtiter plates were constantly shaking at 150 rpm. LB growth rates were first assessed by
648 manual fitting of a line to the exponential phase of the growth curve. This dataset was then
649 used to confirm the accuracy of R code that calculated the fastest growth rate from each
650 growth curve using a "sliding window" approach where a line was fit to a 3-9 timepoint
651 interval based on the level of noise in the entire curve (higher levels of noise triggered a larger
652 window to smooth the fit). To develop an automated method of analyzing the ASM growth
653 curves, which are much more noisy and irregular than the LB growth curves across the
654 collection, we used standardized metrics for identifying problematic curves that we then also
655 evaluated visually. Curves with a maximum OD increase of less than 0.05 were discarded as
656 non-growing. Curves with linear fits with an R^2 of less than 0.7 were discarded as non-
657 analyzable, and a small number of outlier curves (defined as curves analyzed for growth rates
658 of 1.5 times the mean strain growth rate) were also discarded. Examples of our analyzed
659 curves are shown in Figure S7 and all visualizations are available upon request.

660

661 ### "Adherence" measures

662 The ability to form biofilm is a complex trait that is impacted by multiple factors, such as the
663 production of polysaccharides, motility and the ability to adhere [56–58]. In this study, we have
664 measured adhesion to peg-lids and estimated the ability to make aggregates – both traits
665 have been linked with an isolate's ability to make biofilm [59,60]. Because of this, we are using
666 these two measures as an estimate of our isolates' ability to make biofilm. However, because
667 we are aware of the complexity of the actual biofilm-forming phenotype, we have chosen to
668 refer to this adhesion/aggregation phenotype as "adherence" and not "biofilm formation".

669

670 *Adhesion in LB.* Adhesion was estimated by measuring attachment to NUNC peg lids. Isolates
671 were re-grown in 96 well plates with 150µl medium where peg lids were used instead of the
672 standard plate lids. The isolates were incubated for 20 hours at 37°C, after which OD_{600nm} was
673 measured and subsequently, the peg lids were washed in a "washing microtiter plate" with
674 180µl PBS to remove non-adhering cells. The peg lids were then transferred to a microtiter
675 plate containing 160µl 0.01% crystal violet (CV) and left to stain for 15 min. The lids were then
676 washed again three times in three individual "washing microtiter plates" with 180µl PBS to
677 remove unbound crystal violet. To measure the adhesion, the peg lids were transferred to a
678 microtiter plate containing 180µl 99% ethanol, causing the adhering CV stained cells to detach
679 from the peg lid. This final plate was used for measurements using an ELISA reader, measuring
680 the CV density at OD_{590nm}. (Microtiter plates were bought at Fisher Scientific, NUNC Cat no.
681 167008, peg lids cat no. 445497)
682
683 *Aggregation in ASM.* Aggregation in each well was first screened by visual inspection of wells
684 during growth assays in ASM and by evaluation of noise in the growth curves, resulting in a
685 binary metric of "aggregating" versus "not aggregating". However, to incorporate this trait in
686 our archetype analysis, we needed to develop a continuous metric of aggregation. Based on
687 the above manual assessment, we developed a metric based on the average noise of each
688 strain's growth curves. While we tested several different metrics based on curve variance, the
689 metric that seemed to delineate isolates according to the binary aggregation measure most
690 successfully was based on a sum of the amount of every decrease in OD that was followed by
691 a recovery at the next time point (versus the expected increase in exponential phase and
692 flatline in stationary phase). This value was normalized by the increase in OD across the whole
693 growth curve, to ensure that significant, irregular swings stood out with respect to overall
694 growth. This metric therefore specifically accounts for fluctuation - both a limited number of
695 large fluctuations in OD_{630nm} (often seen during stationary phase) as well as smaller but
696 significant fluctuations across the entire curve (i.e. sustained irregular growth). While an
697 imperfect assay of aggregation compared to available experimental methods [61], this high-
698 throughput aggregation estimate showed a significant relationship with adhesion when
699 analyzed with GAMMs (Figure 3D), supporting its potential as a measure of adherence-linked
700 behavior. We show examples of the measurement and comparison with binary aggregation
701 data in Figures S7-8.

702

703 ## Protease production

704 Protease activity was determined using 20x20 cm squared LB plates supplemented with 1.5%
705 skim milk. From a "master microtitre plate", cells were spotted onto the square plate using a
706 96 well replicator. Colonies were allowed to grow for 48h at 37°C before protease activity,
707 showing as a clearing zone in the agar, was read as presence/absence.

708

709 ## Mucoidity

710 Mucoidity was determined using 20x20 cm squared LB plates supplemented with 25 ug/ml
711 ampicillin. From a "master microtitre plate", cells were spotted onto the square plate using a
712 96 well replicator. Colonies were allowed to grow for 48h at 37°C before microscopy of colony
713 morphologies using a 1.25x air Leica objective. By this visual inspection, it was determined if
714 a colony was mucoid or non-mucoid.

715

716 ## MIC determination of ciprofloxacin and aztreonam

717 MICs were determined by E-tests where a suspension of each isolate (0.5 McFarland
718 standard) was inoculated on 14 cm-diameter Mueller-Hinton agar plates (State Serum
719 Institute, Hillerød, Denmark), where after MIC E-Test Strips were placed on the plate in
720 accordance with the manufacturer's instructions (Liofilchem®, Italy). The antimicrobial
721 concentrations of the E-tests were 0.016-256µg/ml for aztreonam and 0.002-32µg/ml for
722 ciprofloxacin.

723

724 ## Construction of *gyrA/B* mutants

725 Four *P. aeruginosa* PAO1 mutants carrying point mutations in *gyrA* and *gyrB* were
726 constructed: PAO1::$gyrA^{G259A}$, PAO1::$gyrA^{C248T}$, PAO1::$gyrB^{C1397T}$, and PAO1::$gyrB^{G1405T}$. A
727 recombineering protocol optimized for *Pseudomonas* was adapted from Ricaurte *et al.*
728 (2017)[62]. A PAO1 strain carrying a pSEVA658-ssr plasmid[63] expressing the recombinase *ssr*
729 was grown to exponential phase with 250 rpm shaking at 37°C. Bacteria were then induced
730 with 3-methylbenzoate and electroporated with recombineering oligonucleotides. Cells were
731 inoculated in 5 ml of glycerol-free Terrific Broth (TB) and allowed to recover overnight at 37°C

732 with shaking. Cip^R colonies were identified after streaking on a Cip-LB plate (0.25 mg L^{-1}) and
733 sent for sequencing after colony PCR.
734
735 Each recombineering oligonucleotide contained 45 base pair homology regions flanking the
736 nucleotide to be edited. Oligonucleotides were designed to bind to the lagging strand of the
737 replichore of both genes and to introduce the mismatch in each mutation: G259A and C248T
738 in *gyrA*, and C1937T and G1405T in *gyrB*, respectively. The recombineering nucleotides used
739 are the following: (Rec_gyrA_G259A -
740 G*C*ATGTAGCGCAGCGAGAACGGCTGCGCCATGCGCACGATGGTGTtGTAGACCGCGGTGTCGCC
741 GTGCGGGTGGTACTTACCGATCACG*T*C; Rec_gyrA_C248T -
742 A*G*CGAGAACGGCTGCGCCATGCGCACGATGGTGTCGTAGACCGCGaTGTCGCCGTGCGGGTGGT
743 ACTTACCGATCACGTCGCCGACCAC*A*C; Rec_gyrB_C1397T -
744 C*C*GATGCCACAGCCCAGGGCGGTGATCAGCGTACCGACCTCCTGGaAGGAGAGCATCTTGTCGA
745 AGCGCGCCTTTTCGACGTTGAGGAT*C*T; Rec_gyrB_G1405T
746 C*C*TCGCGGCCGATGCCACAGCCCAGGGCGGTGATCAGCGTACCGAaCTCCTGGGAGGAGAGCAT
747 CTTGTCGAAGCGCGCCTTTTCGACG*T*T).
748

749 ## Modeling of phenotypic evolution

750 To identify patterns of phenotypic adaptation while limiting necessary model assumptions
751 that might bias our predictions, we chose to implement generalized additive mixed models
752 (GAMMs), where the assumptions are that functions are additive and the components are
753 smooth. These models allow us to account for patient-specific effects, thereby enabling us to
754 identify trends in phenotypic adaptation across different genetic lineages and different host
755 environments. Furthermore, to be able to simultaneously assess multiple phenotypes of each
756 isolate from a systems perspective, we implemented archetype analysis (AA), where each
757 isolate is mapped according to its similarity to extremes, or archetypes, fitted on the
758 boundaries of the multi-dimensional phenotypic space. This modeling approach allows us to
759 predict the number and characteristics of these archetypes and furthermore identify
760 distinctive evolutionary trajectories that emerge from longitudinal analysis of fitted isolates
761 for each patient.
762

763 For all analyses, the time of infection is defined within each lineage as the time since the clone
764 type of interest was first discovered in the patient in question. This is biased in the sense that
765 the time since colonization can only be calculated from the first sequenced isolate of a
766 patient. However, we have collected and sequenced the first isolate that has ever been
767 cultured in the clinic for 20 out of the 39 patients.
768
769 Normalization of phenotypic values were carried out the following way for both AA and
770 GAMM: ciprofloxacin and aztreonam MICs were normalized by dividing the raw MICs with
771 the breakpoint values from EUCAST: ciprofloxacin breakpoint value: >0.5 µg/ml, aztreonam
772 breakpoint value: >16 µg/ml (EUCAST update 13. March 2017). This results in values above
773 one equaling resistance and equal to or below one equaling sensitive. The response and the
774 explanatory variables were log2 transformed to get a better model fit for ciprofloxacin MIC,
775 aztreonam MIC, Adhesion, and Aggregation. For the AA, Adhesion, Aggregation and growth
776 rate in ASM was further normalized (before log2 transformation) by scaling the values by the
777 values of the laboratory strain *P. aeruginosa* PAO1 such that zero was equivalent to the PAO1
778 phenotype measurement or the EUCAST MIC breakpoint. PAO1 was chosen to be the
779 reference point of "wild type" phenotypes.
780
781 Because the mutations identified in our collection are based on our previous study [16] where
782 mutations were called within the different clone types, we added a second filtering step to
783 identify mutation accumulation within patients. The second filtering step removed mutations
784 present in all isolates of a lineage (a clone type within a specific patient) from the analysis.
785
786 All statistics were carried out in R[64] using the packages *mgcv*[65,66] for the GAMM analysis and
787 *archetype*[67–69] for the AA. Complementary packages used for analysis are: *tidyverse*[70],
788 *itsadug*[71], *ggthemes*[72], *knitr*[73] and *kableExtra*[74]. We also referred to Thøgersen *et al.*[27] and
789 Fernandez *et al.*[75] in the design of appropriate assessment methods for the final AA model.
790 We include two R markdown documents that explain our modeling steps and further
791 evaluation plots in detail (AA: Supplemental file 1, GAMM: Supplemental file 2), and
792 summarize our methods below in brief.
793

794 Data modeling

795 *Archetype analysis (AA).* We evaluated several different model fitting approaches by varying
796 the number and type of phenotypes modeled as well as the archetype number and fit
797 method, using RSS-based screeplots of stepped fits of differing archetype numbers, explained
798 sample variance (ESV), isolate distribution among archetypes, convex hull projections of
799 paired phenotypes (all combinations), and parallel coordinate plots as metrics for choosing
800 the best fit parameters and approach to accurately represent our data. Ultimately, we
801 focused on 5 continuous phenotypes correlated with growth (growth rate in ASM), biofilm
802 (adhesion and aggregation), and antibiotic resistance (aztreonam and ciprofloxacin MICs),
803 which also were linked to relevant findings provided by the GAMM models. We used a root
804 sum squared (RSS) versus archetype number screeplot of different fits to determine that a 6
805 archetype fit would produce the optimal model for this dataset.

806

807 We then performed 500 simulations of a 100 iteration fit using the "robustArchetypes"
808 method[68], which reduces the impact of data outliers in fitting the convex hull of the data. We
809 evaluated the mean ESV and the number of isolates with an ESV greater than 80% for the best
810 model from each simulation in this study and differences in archetype characteristics to
811 assess convergence, ultimately selecting the model with the second highest mean ESV
812 (90.32%) and highest number of isolates with an ESV over 80% (87.13%); this model also
813 resembled the other 10 top models of the simulation study. The order of archetypes around
814 the simplex plot boundary obscures the true dimensionality of the isolate distribution by
815 implying the archetypes are equidistant, so relationships between phenotypes are not always
816 obvious. We re-ordered the archetypes in the simplex plot by growth rate and secondarily
817 antibiotic resistance to improve clarity in the complex 6 archetype plot. This reordering was
818 also justified when projecting the archetypes onto a PCA plot of the phenotypes
819 (Supplemental file 1). All simplex plots have also had the 11 isolates with an ESV < 50%
820 removed such that we are not drawing any conclusions from these poorly fit data (they are
821 shown via simplex plot in the supplemental markdown).

822

823 *Generalized Additive Mixed Models (GAMMs).* For all phenotypes, GAMMs were used to
824 identify evolutionary trends over time since first colonization. We correct for the patient
825 environment and inconsistent sampling over time using a smooth random factor. Models

826 were fitted in the following way: All continuously measured phenotypes included in the
827 Archetype analysis were fitted as a response variable (”predicted” or “dependent” variable in
828 Figure 3D) one-to-one, with both time as an “explanatory” or “independent” variable alone
829 and combined with each of the phenotypes to account for potential time-dependence of the
830 observations. Factorial/binary phenotypes were implemented as categorical functions and
831 continuous phenotypes as smooth functions, allowing for non-parametric fits. Normally only
832 one variable/phenotype of interest is used as the predictor while other alterable variables or
833 factors are used as explanatory variables to explain or predict changes in the predictor.
834 However, this requires a preconceived idea of a “one-way-relationship” where one variable
835 (the predictor) is assumed to be affected by certain other variables (the explanatory
836 variables), but where the explanatory variables cannot be affected by the predictor. By testing
837 all phenotypes against each other, we avoid assumptions regarding the specific direction of
838 relationships between the predictor variable and the explanatory variable. Furthermore, in
839 using the GAMMs we prioritize accuracy of fitting but increase our risk of overfitting as a
840 byproduct. We sought to counteract the risk of overfitting by the default penalization of fits
841 inherent to the method used[65,66] and by model estimation via restricted maximum likelihood
842 (REML) which has been found to be more robust against overfitting[31,66]. When significant
843 relationships were identified in one-to-one models (p-value < 0.05, as based on Wald-type
844 tests as described in[31,32]), all significant explanatory variables were used to build a multi-trait
845 model for the associated predictor. If select explanatory phenotypes were then identified as
846 non-significant (p-value > 0.05) in the multi-trait model, they would be removed in a reduction
847 step. To identify whether a reduced multi-trait model resulted in a better fit than the initial
848 multi-trait model, a Chi-square test was carried out on the models using the compareML
849 function of the R package *itsadug*[71] (Figure 3D). The specific models and additional
850 information can be found in Supplemental file 2.
851
852 In demonstration of the utility of this approach, the multi-trait models of our 5 primary
853 predictor phenotypes show that at least one explanatory phenotype has a statistically
854 significant impact on the predictor phenotype. For all of the predictor phenotypes, multiple
855 explanatory traits preserved significant impacts after model reduction steps (Figure 3D and
856 Supplemental file 2). All mentions of significant relationships or correlations in the main text
857 are obtained from the GAMM analyses with Wald-type test statistics presenting p-values <

858 0.01, unless otherwise stated. For information on deviance explained, R^2, and degrees of
859 freedom for the individual models/variables, we refer to the Supplemental file 2.
860

861 SUPPLEMENTARY INFORMATION

862 Supplemental File 1. Construction and assessment of the archetype model.
863 Supplemental File 2. Construction and assessment of the generalized additive mixed models.
864 Supplemental spreadsheet 1. Phenotype Database
865 Supplemental Information.
866 Figure S1, related to Figure 4. Hypermutators versus normomutators
867 Figure S2, related to Figure 5. *mucA* and *algU* mutants
868 Figure S3, related to Figure 5. mexZ mutants and drug efflux pumps
869 Figure S4, related to Figure 5. Specific mutations in *gyrA/B* by patient and adhesion
870 Figure S5, related to Figure 5. Adhesion and generation time of *gyrA/B* mutants (PAO1)
871 Figure S6, related to Figure 2. Example growth curves
872 Figure S7, related to Figure 2. Development of an aggregation metric
873